Dynamic behaviour of drystone retaining walls: shaking table scaled-down tests

N Savalle, J Blanc-Gonnet, E Vincens, S Hans

Dynamic behaviour of drystone retaining walls: shaking table scaled-down tests

N. Savalle[a], J. Blanc-gonnet[b], E. Vincens[a] and S. Hans[b]

[a]Université de Lyon, LTDS, UMR CNRS 5513, École Centrale de Lyon, 36 Avenue Guy de Collongue, 69134 Écully Cedex, France
[b]Université de Lyon, LTDS, UMR CNRS 5513, École Nationale des Travaux Publics de l'État, 3 rue Maurice Audin, 69518 Vaulx en Velin Cedex, France

ARTICLE HISTORY
Compiled December 5, 2020

The Version of Record of this manuscript has been published and is available in European Journal of Environmental and Civil Engineering. 24th November 2020.
DOI: http://www.tandfonline.com/10.1080/19648189.2020.1855477

ABSTRACT
In this paper, an experimental study aiming at understanding the seismic behaviour of dry stone retaining walls is presented. Harmonic shaking table tests have been carried out on scaled-down dry-joint retaining walls involving parallelepiped bricks. It is found that a thicker wall is more resistant and that a given retaining wall is less sensitive to higher frequencies. For those higher frequencies, the walls accept larger displacements before collapsing. The displacements start to occur from a given threshold, which depends on the wall geometry but not on the frequency of the base motion. The typical toppling failure is observed for slender wall and/or low frequency inputs. For less slender walls or higher frequency inputs, walls experience local sliding failures until the complete collapse of the system. The acceleration at failure reported during the dynamic tests have been compared to the corresponding pseudo-static resistance, enabling a conservative estimate of the seismic behaviour coefficient for pseudo-static analysis of this class of retaining walls. This novel experimental dataset is aimed to serve as a validating framework for future numerical or analytical tools in the field.

KEYWORDS
Earthquake engineering; masonry; shaking table tests; dry stone; seismic behaviour; harmonic shaking; DSRW

1. Introduction

Dry stone retaining walls (DSRWs) are present worldwide and constitute an important cultural heritage for numerous territories. Today, this old heritage is generally damaged due to weathering but also due to a lack of maintenance. In France, most of the DSRWs have been erected before World War I and no more walls were built after World War II. Since this damaged heritage can be considered as an economical asset for these territories (tourism, agriculture, transportation), the local authorities have some great concerns in relation to their conservation. The required interventions on this heritage are however difficult to make in a context where the behaviour of DSRWs is not completely known.

A lot of studies have been carried out on DSRWs since the first known experimental work performed by Lieutenant Sir John Burgoyne in 1834 (Burgoyne, 1853) who studied the impact of the section geometry on

CONTACT E. Vincens. Email: eric.vincens@ec-lyon.fr

The Version of Record of this manuscript has been published and is available in European Journal of Environmental and Civil Engineering. 24th November 2020.
DOI: http://www.tandfonline.com/10.1080/19648189.2020.1855477

the resistance of DSRWs. These first experiments have been afterwards modelled using analytical methods (Husband & Harby, 1911; Capper & Cassie, 1969; Clayton et al., 2014) or numerical models using the Discrete Element Method (DEM) (Harkness et al., 2000; Powrie et al., 2002; Claxton et al., 2005). At the time, DEM codes had already been used to successfully model the free standing walls of Great Zimbabwe site (UNESCO) (Walker & Dickens, 1995; Dickens & Walker, 1996). Further experiments on slope DSRWs were carried out much more recently when Villemus et al. (2006) and Colas et al. (2010, 2013a) aimed at finding the critical height of a backfill that triggers the collapse of a DSRW. They developed analytical methods (Villemus et al., 2006; Colas et al., 2008, 2013b) to create charts included in design guides for the French dry stone masons (CAPEB et al., 2008; ENTPE et al., 2017). These works have been complemented by analytical refinements (Terrade et al., 2018) as well as more sophisticated numerical models (Oetomo et al., 2016). In other European countries, the behaviour of slope DSRWs is also a new field of research (Walker et al., 2007; Alejano, Veiga, Gómez-Márquez, & Taboada, 2012; Alejano, Veiga, Taboada, & Díez-Farto, 2012; Pulatsu et al., 2020). In addition, other experimental (Mundell et al., 2009, 2010; McCombie et al., 2012; Le et al., 2019), analytical (Le et al., 2016) and numerical (Quezada et al., 2016) studies have been carried out on 3D failure of DSRWs induced by a concentrated load on backfill top.

All these studies focused on the static behaviour of DSRWs. However, the assessment of the seismic stability of these structures is a necessary step to guide the repair of old structures, as well as to design new ones, since they may be located in seismic zones. Fukumoto et al. (2014) carried out an experimental study on the seismic behaviour of DSRWs but focused on the optimal shape of dressed stones for the wall seismic resistance through centrifuge scaled-down tests. A pseudo-static study on slope DSRWs was carried out by Savalle et al. (2018a) and Savalle et al. (2018b) with the aim at developing a practical analytical tool for the design of DSRWs in seismic areas. Although seismic recommendations are given for the design of slope DSRWs in low seismic risk zones, their method failed to give realistic recommendations for higher seismic risk zones, as pseudo-static approaches are known to be over conservative in that case (Richards & Elms, 1979; Bellezza, 2014; Savalle et al., 2018a), thus requiring a displacement design approach (Newmark, 1965; Huang et al., 2009; Gaudio et al., 2018). Therefore, dynamic approaches must be followed to get a better insight into the seismic behaviour of slope DSRWs.

Dynamic studies using shaking table tests are common in geotechnical engineering: numerous studies of slope stability (Sugimoto et al., 1994; Bathurst et al., 2002; Lo Grasso et al., 2004; Huang et al., 2010; Srilatha et al., 2013) and of unreinforced (or reinforced) retaining walls (Ishibashi & Fang, 1987; Fairless, 1989; Iai, 1989; Koseki et al., 1998; Bathurst et al., 2002; Bathurst, 2002; Huang et al., 2009; Wilson & Elgamal, 2015) have been carried out in the past thirty years. However, none of them dealt with the specificity of DSRWs, where blocks can move during the base motion and hence can dissipate energy before collapsing.

In order to pave the way to numerical and analytical dynamic studies, a vast and novel experimental campaign of shaking-table tests involving dry stone retaining walls is envisioned in this work. First, shaking table tests on scaled-down dry-joint brick retaining walls are presented. Then, the influence of the slenderness of the wall as well as the frequency of the ground motion on the behaviour of the retaining walls are investigated. Finally, a comparison with pseudo-static calculations is conducted and a conservative value for the seismic behaviour coefficient r is proposed.

2. Experimental set-up

2.1. Shaking-table tests

2.1.1. Principle of the tests

Herein, more than forty tests on a shaking table have been carried out using scaled-down models of dry-joint brick walls retaining a sandy backfill. The walls were erected using small paralelepiped shaped clay bricks. The mock-up was loaded by a horizontal harmonic ground motion whose amplitude was increased from 0 until the collapse of the wall.

One could note that the parallelepiped bricks utilised in this work are quite different in shape from the undressed blocks used in the field. This latter point has already been studied by other authors. First, Fukumoto et al. (2014) found that, using a trapezoidal shape for stones, the results of centrifuge tests were actually improved compared to more simple shapes like parallelepipeds. However, they attributed this improvement to the change in the backfill-wall interface friction angle and not directly to the shapes of stones. In addition, all numerical and analytical static studies modelling the actual irregular blocks by parallelepiped blocks have been proved relevant to found the key parameters driving the behaviour of actual dry stone walls as well as their ultimate capacity (Dickens & Walker, 1996; Harkness et al., 2000; Powrie et al., 2002; Claxton et al., 2005;

The Version of Record of this manuscript has been published and is available in European Journal of Environmental and Civil Engineering. 24th November 2020.
DOI: http://www.tandfonline.com/10.1080/19648189.2020.1855477

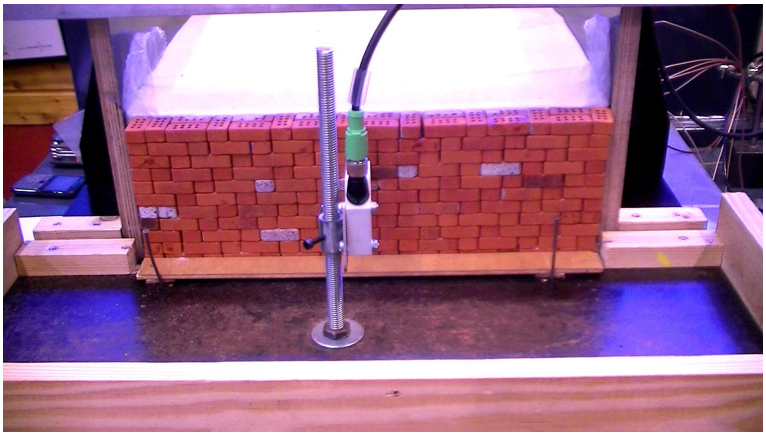

Figure 1. Mock-up of the dry joint retaining wall before a shaking-table test.

Villemus et al., 2006; Colas et al., 2008; Mundell et al., 2009; Colas et al., 2013b; Oetomo et al., 2016; Savalle, 2019; Pulatsu et al., 2020). It means that, as long as the dry stone walls are constructed following the state of the art of dry stone construction, the shape of the blocks does not seem to play a significant role on the wall stability.

2.1.2. Experimental devices

The erected retaining walls were B = 34mm wide, L = 400mm long and H = 50 to 140mm high and were made of clay bricks of dimensions: height×width×length = 11mm×17mm×34mm. They were placed in the aperture of a container of dimensions height×width×length = 250mm×400mm×400mm (*Figure 1*). To reduce the significance of the two walls ends (potentially the most vulnerable parts), the wall length L has been chosen sufficiently large. Indeed, according to Dewoolkar et al. (2000), above a wall ratio L/H = 2.0, end effects do not alter the plane strain conditions.
The backfill was made of a dry Hostun sand S28[1], filling the container and having an equivalent volume of height×width×length = 50-140mm×400mm×400mm (*Figures 1* and *2*). Using an analytical pseudo-static approach, the backfill width W (*Figure 2*) was designed so that the failure surface in the backfill did not interfere with the vertical back wall of the container (Savalle et al., 2018a). This aspect was validated throughout the shaking-table tests.

The whole mock-up (30-60kg) was placed on an electrodynamic shaking table of dimensions 60cm×60cm that can handle accelerations of 8g for loads of 600N, (Serial number: Sonic S201LS3-340/SPA203). In order to absorb harmonic waves reaching or originated from the vertical back wall of the container, this latter was covered by an absorbing foam which was intended to reproduce free-field conditions (*Figure 2*). Moreover, a gap was introduced between the brick wall ends and the lateral container walls to avoid any disturbing friction at this location. Two plastic sheets were placed in this gap to prevent the seepage of the backfill sand (*Figure 1*). The first layer of the wall was fixed in order to model a rigid foundation with an infinitely resistant abutment (*Figures 1* and *2*). In the following, the wall height (H) refers to the height of the free wall and does not take into account this first fixed layer. Therefore, the base friction of the wall was the one of the brick-brick contact itself. In addition, a Linear Variable Displacement Transducer (LVDT6 in *Figure 2*) was used to monitor the settlement of the backfill. Then, a laser sensor (serial number: FT 50 RLA-40-F-L4S of SensoPart company) was used to measure the displacement of the second to last row of bricks. It will be used later as an indicator of failure for the wall.

Finally, eight accelerometers (ACC) with a minimum precision of 10mV/g have been placed at different locations on the container to quantify its 3-dimensional dynamic response (*Figure 2*). The accelerometer labeled ACC2, located on the floor of the container, was a special low-frequencies sensor that has been used as an input for the shaking-table tests (special precision of 1000mV/g). The accelerometer labeled ACC10 was a triaxial sensor and all the other sensors (ACC3, ACC4, ACC5, ACC7, ACC8, and ACC9) were mono-directional and oriented in the direction of shaking ($\vec{X}$), perpendicular to the wall face (*Figure 2*).

[1]The S28 sand had minimum and maximum void ratios equal to e_{min} = 0.689 and e_{max} = 1.031 (Combe, 1998).

The Version of Record of this manuscript has been published and is available in European Journal of Environmental and Civil Engineering. 24th November 2020.
DOI: http://www.tandfonline.com/10.1080/19648189.2020.1855477

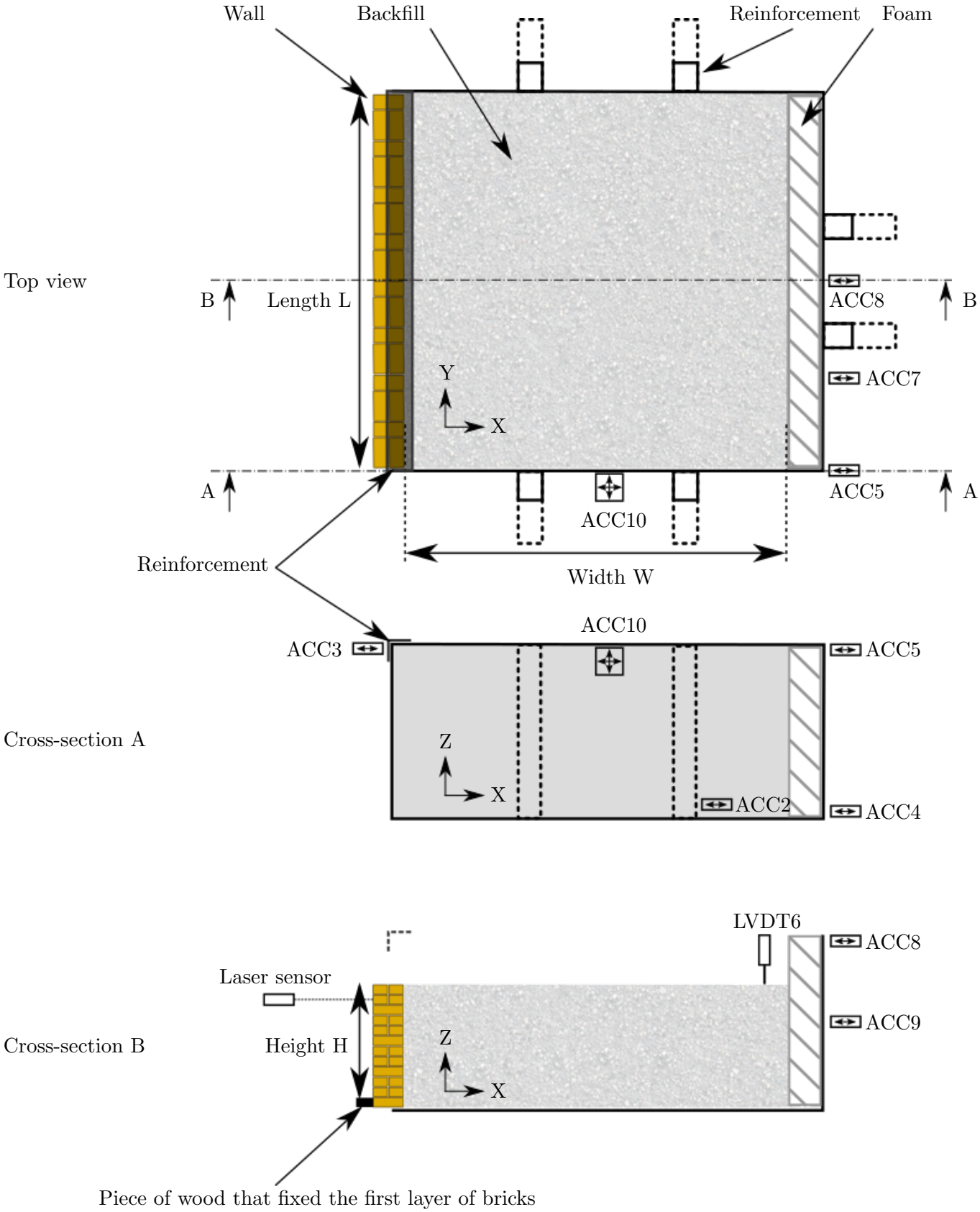

Figure 2. Scheme of the mock-up (top and cross-section views). Accelerometers (ACC), laser sensor and Linear Variable Displacement Transducer (LVDT) are depicted.

The Version of Record of this manuscript has been published and is available in European Journal of Environmental and Civil Engineering. 24th November 2020.
DOI: http://www.tandfonline.com/10.1080/19648189.2020.1855477

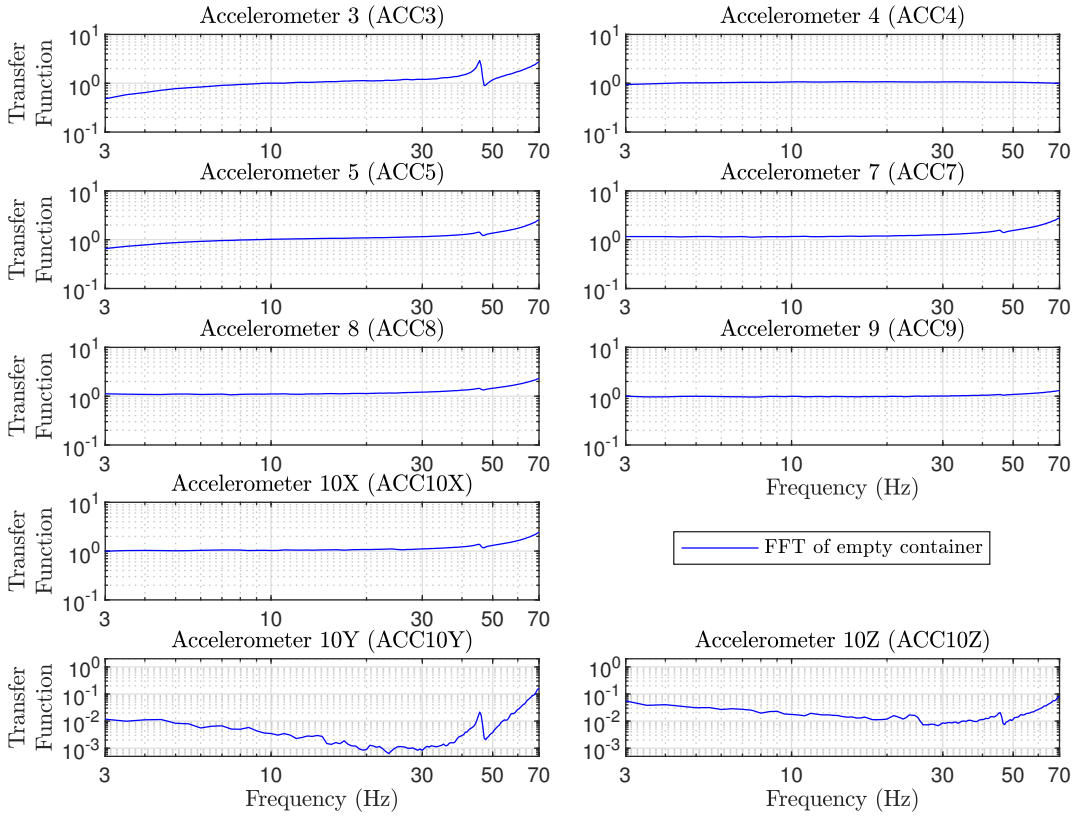

Figure 3. White noise response of the empty container. Transfer Functions (normalized by the input signal) of the signal received by the accelerometers.

2.2. Experimental protocol

2.2.1. Preliminary results

It has been observed that the container had not a simple response with neither fully rigid nor fully deformable pattern which would not make future numerical simulations easy. Then, an analysis of the response of the container is presented in this part.

Using a white noise input signal given to the base of the model (ACC2), the Transfer Functions[2] of the responses of all other accelerometers have been analysed (*Figure 3*). Though only the response of the empty container is shown, the response of the container filled with different backfill heights (5cm, 8cm, 10cm, 15cm and 20cm) has been found similar. It is observed that in the range of frequencies between 10Hz and 30Hz, the container can be likened to a rigid container. Indeed, all accelerometers in the X-direction (ACC3, ACC4, ACC5, ACC7, ACC8, ACC9 and ACC10X) had a frequency response equal to the one of the input signal, while there were no junk vibrations in the other directions (ACC10Y and ACC10Z). Analysing the data from sensors ACC4 and ACC9 (not placed at the top of the container), and considering that the top surface of the backfill was never above the sensor ACC9, the mock-up can be considered as rigid up to the investigated frequency of 70Hz.

Then, the response of the backfill itself has been studied. The first resonant frequency of the backfill layer has been evaluated using the classical free-field shear layer model of soils which gives the frequency of the first mode:

$$f_0 = \frac{C_s}{4H} \tag{1}$$

[2]The Transfer Function corresponds to the Fourier Transform of the response of an accelerometer divided by the Fourier Transform of the input signal (ACC2), which is herein characterised by a plateau between 3Hz and 70Hz.

The Version of Record of this manuscript has been published and is available in European Journal of Environmental and Civil Engineering. 24th November 2020.
DOI: http://www.tandfonline.com/10.1080/19648189.2020.1855477

with H the height of the backfill and C_s the speed of shearing waves in the backfill, given by

$$C_s = \sqrt{\frac{G}{\rho}} = \sqrt{\frac{\frac{E}{2(1+\nu)}}{\rho}} \tag{2}$$

with G the shear modulus of the sand, E its Young's modulus, ν, its Poisson's ratio and ρ its unit mass. The elastic modulus $E = 18$MPa was evaluated using the formula from Biarez and Hicher (1994), $e = 0.72$ being the sand's void ratio and $p' = 0.7$kPa the confining pressure:

$$E \text{ (in MPa)} = \frac{450}{e} \times \sqrt{p' \text{ (in MPa)}} \tag{3}$$

Using a classical Poisson's ratio of $\nu = 0.3$, a backfill height H ranging between 5cm and 15cm and the experimental unit weight of $\rho = 1540\text{kg.m}^{-3}$, the first eigen-frequency of the backfill is expected to range between 100Hz and 300Hz. In addition, one should note that the validity of *Equation 3* for low confined soil is not established. Indeed, close to the soil surface, this equation predicts an excessively deformable material which does not hold any physical meaning. Therefore the actual value might be larger than the predicted one. Therefore, even at 70Hz, the resonance of the sand layer is not likely to be triggered throughout the experiments. However, this aspect could not have been checked, since the precision of the laser sensor (≈ 0.1mm) was too poor compared to the amplitude of the signal (≈ 0.01mm at 70Hz).

2.2.2. Description of the protocol

First, the wall was erected in the aperture of the container. Then, the sand was carefully deposited from a zero drop-height in order to obtain an homogeneous loose backfill. As the backfill was expected to settle due to the subsequent shakings, a preliminary step for all shaking-table tests was applied to stabilise it to a final state, turning the loose backfill into a dense backfill[3]. It consisted in applying a five-minutes duration white noise to the wall-backfill system (constant spectral density of $0.001\text{g}^2/\text{Hz}$ in the range of [3-300Hz] leading to a mean acceleration of 0.6g). This white noise input has been found sufficient to achieve a dense and stable state for the backfill, that would not evolve afterwards. The wall was maintained in place by a wood panel fixed to the container, so that no failure of the wall could happen throughout this preliminary stage.

An actual seismic signal is a combination of multiple harmonic waves, whose amplitude is varying in time but also in frequency. In a research context, this complex motion needs to be first simplified in order to understand the basic dynamic features, instead of using actual earthquake recordings where the influence of all parameters is difficult to extract. Therefore, in a first step, the authors chose harmonic waves as input motions in the shaking-table tests, before more complex signals that will be addressed in a future work. Four frequencies compatible with the response of the container have been used (*Figure 3*): 10Hz, 30Hz, 50Hz and 70Hz, which is in accordance with the classical frequency scaling law given by (Ishibashi & Fang, 1987; Krawinkler, 1988; Fairless, 1989; Huang et al., 2010):

$$f_{\text{scaled-down}} = f_{\text{full-scale}} * \sqrt{\frac{1}{K}} \tag{4}$$

where $f_{\text{scaled-down}}$ is the frequency of shaking in the scaled model, $f_{\text{full-scale}}$ is the frequency of shaking at full scale and K is the scale ratio (approximately equal to $1/20 = 0.05$ in these experiments). Given that seismic central frequencies mainly range between 1Hz and 20Hz, one ends up with scaled frequencies between 4.5Hz and 89.4Hz, which is close to the chosen frequency range [10-70Hz].

The equation of the harmonic ground motion $S(t)$ is given by:

$$S(t) = A \times t \times \sin(\omega t) \tag{5}$$

with A a constant (see *Appendix A* for details about its values), t the time throughout the experiment and ω the angular frequency defined as $\omega = 2\pi f$, f being the frequency of the motion (*Figure 4*). The duration of the tests was 30 seconds, which is a typical, though long, duration for an actual quake.

2.3. Material properties of the mock-up

Retaining brick walls had a width of $B = 34$mm and a variable height H (50mm to 140mm), enabling the slenderness of the studied walls to range between 1.3 and 4. Only one wall has been erected using a bigger width: $B = 51$mm and a height of $H = 104$mm. A typical assemblage is presented in *Figure 5*. The detailed

[3]Mean void ratios and relative densities of $e_{loose} = 0.97$, $R_{D,\ loose} = 19\%$, $e_{dense} = 0.72$ and $R_{D,\ dense} = 91\%$ have been found throughout the tests.

The Version of Record of this manuscript has been published and is available in European Journal of Environmental and Civil Engineering. 24th November 2020.
DOI: http://www.tandfonline.com/10.1080/19648189.2020.1855477

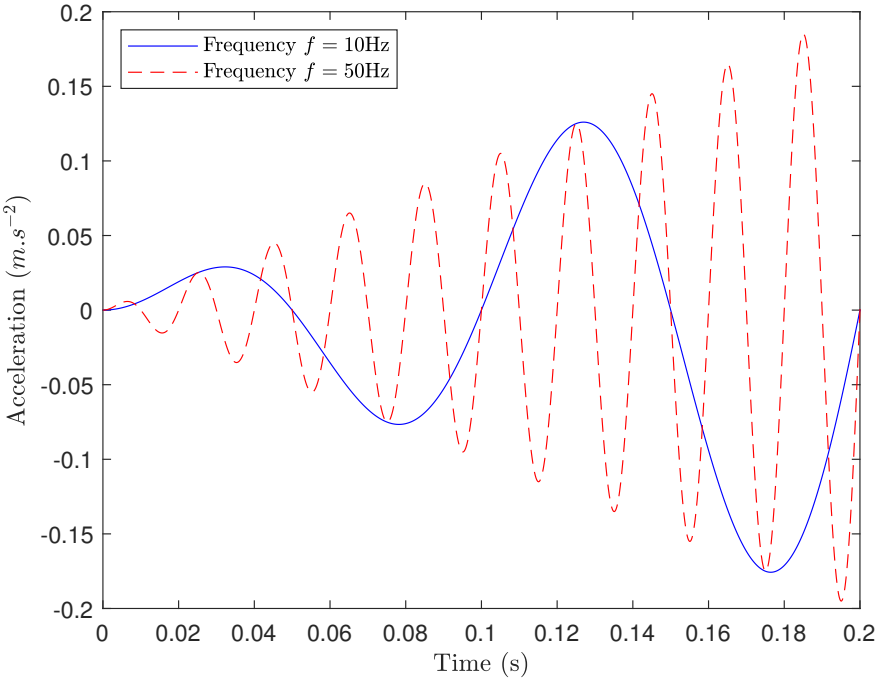

Figure 4. Input acceleration signal S at the base of the model: two frequencies are partially shown (total duration is $\approx$ 30s). The amplitude of the signal increases linearly.

assemblages used to construct the walls can be found in Savalle et al. (2020). They were based on dry stone state-of-art rules and enabled stable masonries: headers were placed frequently and all the bricks were installed with staggered joints.

In this study, the mechanical parameters were derived from previous experimental works that used the same materials (Amirouche, 2008; Quezada et al., 2016; Savalle et al., 2018a). Table 1 gives all the data in relation to the materials. The mean unit weight of the wall as well as the unit weight of the backfill were measured during the experiments and were found to be equal to 14.4kN/m^{-3} and 15.4 $\pm$ 0.1kN/m^{-3} respectively.

The internal friction angle φ'_{sand} of the backfill has been evaluated using several indirect approaches since typical geotechnical tests can hardly be used due to the very low pressures involved in these experiments (approximately $p' = 0.7$kPa at mid-height). Moreover, in the literature there are only few studies focused on low confined sand, and no specific ones on the S28 Hostun sand at dense state. Yet, using literature's analytical expressions and the experimental confining pressure $p' = 0.7$kPa, a value

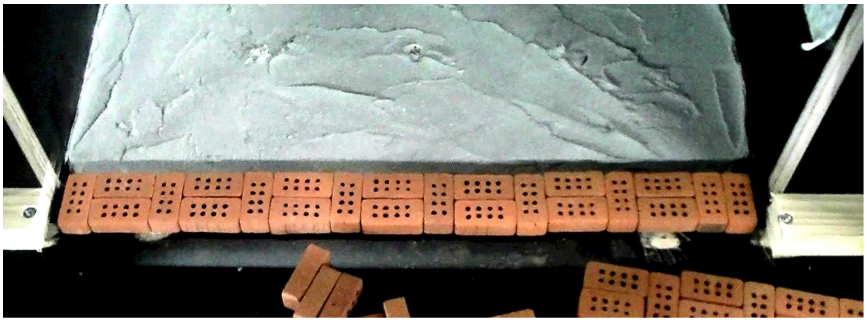

Figure 5. Picture of the assemblage used for each layer: the wall was constructed layer by layer.

The Version of Record of this manuscript has been published and is available in European Journal of Environmental and Civil Engineering. 24th November 2020.
DOI: http://www.tandfonline.com/10.1080/19648189.2020.1855477

Table 1. Mechanical parameters of the experiments. Symbol * refers to Amirouche (2008); symbol $^\diamond$ to Quezada et al. (2016); symbol † to Savalle et al. (2018a) and symbol $^\triangle$ to the present study.

	Brick wall	Dense backfill	Interface	Absorbing foam
Mean unit weight (kN.m^{-3})	14.4 $^\diamond$ † $^\triangle$	15.4 $^\triangle$	-	0.52 *
Friction angle (°)	32° $^\diamond$	45° $^\triangle$	32° †	-
Cohesion (kPa)	0 $^\diamond$	0 $^\triangle$	0 †	-
Damping	-	-	-	0.14 *

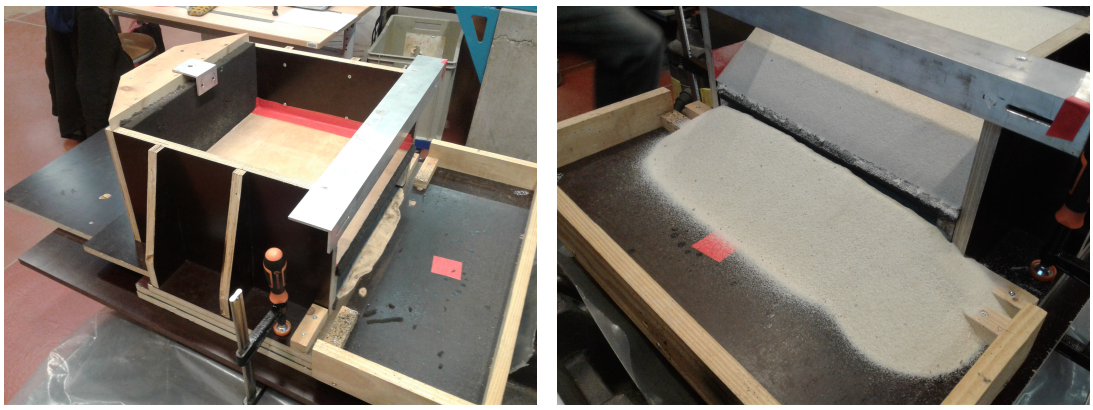

(a) Raised floor without the panel and the backfill (b) Stable slope after removing the panel

Figure 6. (a) A raised floor is added to the container to ensure that (b) the S28 sand that flows falls away from the stable slope.

of $\varphi'_{\text{sand}} = 55°$ can be found (*Appendix B*). Given that this value is out of the range of typical values for this material, two further techniques were envisioned to give an estimate of the internal friction angle φ'_{sand}.

The first one consisted in adding a raised floor (*Figure 6*) and a vertical wood panel instead of the brick wall. After filling the container with the loose sand, the container was shaken by the same white noise as herebefore. Then, while removing the wood panel, a failure surface developed in the backfill and dense sand flowed out of the container. Along this failure surface, it has been observed that the sand experienced strong shearing strains leading to the generation of dilative volumetric strains. Therefore, the obtained sandy slope corresponded to the angle at the critical state which is close to the angle of repose for loose S28 sand (*Figure 6*). Then, a layer (approximately 4cm) of loose sand laying on the dense sand slope (*Figure 7*) was carefully removed with a brush. Out of three different tests, nine measurements of the slope angle were performed leading to an average value of $\varphi'_{\text{sand}} = 45° \pm 2°$.

The second experimental approach consisted in using an inverse method with the help of results coming from a previous study (Savalle et al., 2018a). In that study, an analytical tool was developed to predict the tilting angle at failure of an identical mock-up made of a brick wall retaining a sandy backfill. The only difference arises from the density of the backfill which was in a loose state. To evaluate φ'_{sand}, the container was first filled with the brick wall ($H = 8$cm and $B = 3.4$cm) and with the loose Hostun S28 sand. Then, the preliminary process that lead to a dense backfill was applied. At the end of the shakings, the mock-up was carefully placed on a tilting plateform. After the removal of the vertical wood panel that maintained the brick wall stable, the mock-up was progressively inclined and the tilting angle at failure for the wall was measured. Two tests were carried out for repeatability. Using a trial and error method for the analytical method, the unknown being the internal friction angle of the backfill, values equal to $\varphi'_{\text{sand}} = 41.5°$ and $\varphi'_{\text{sand}} = 43°$ were found. These values are close to the internal friction angle evaluated with the previous experimental approach ($45° \pm 2°$) and are both very different from the one estimated from the literature analysis. Therefore, in the following, an internal friction angle of $\varphi'_{\text{sand}} = 45°$ was considered.

The interface (wall-backfill) friction angle δ_{sand} has not been experimentally evaluated but was deduced

The Version of Record of this manuscript has been published and is available in European Journal of Environmental and Civil Engineering. 24th November 2020.
DOI: http://www.tandfonline.com/10.1080/19648189.2020.1855477

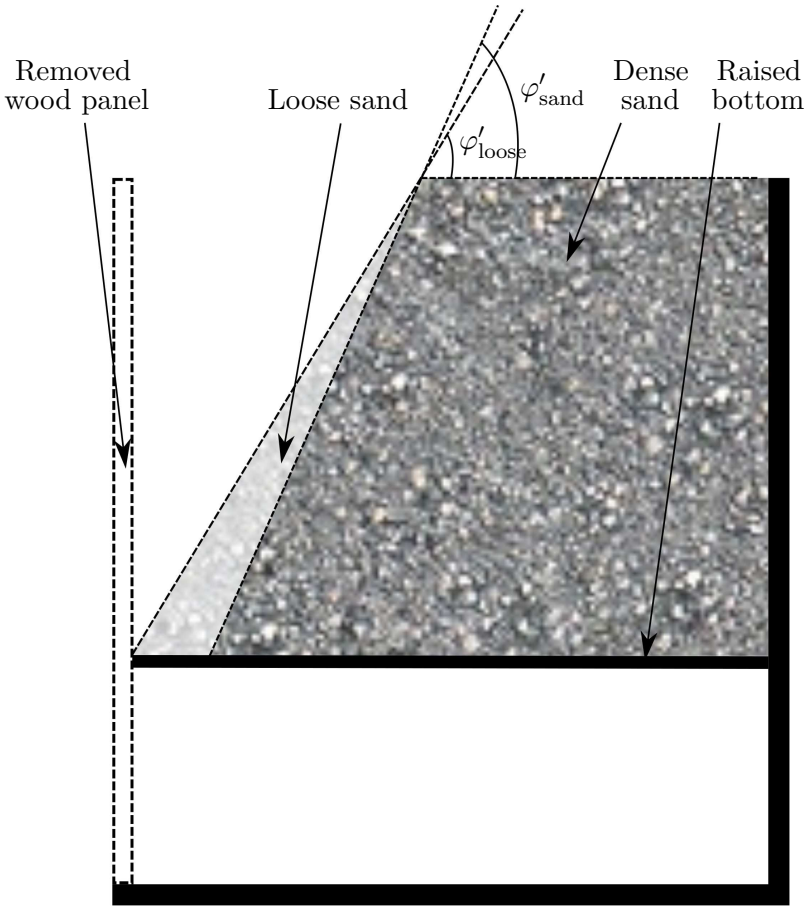

Figure 7. 2D scheme of the stable slope after removing the vertical wood panel. A layer of loose S28 sand stands in front of the dense sand.

The Version of Record of this manuscript has been published and is available in European Journal of Environmental and Civil Engineering. 24th November 2020.
DOI: http://www.tandfonline.com/10.1080/19648189.2020.1855477

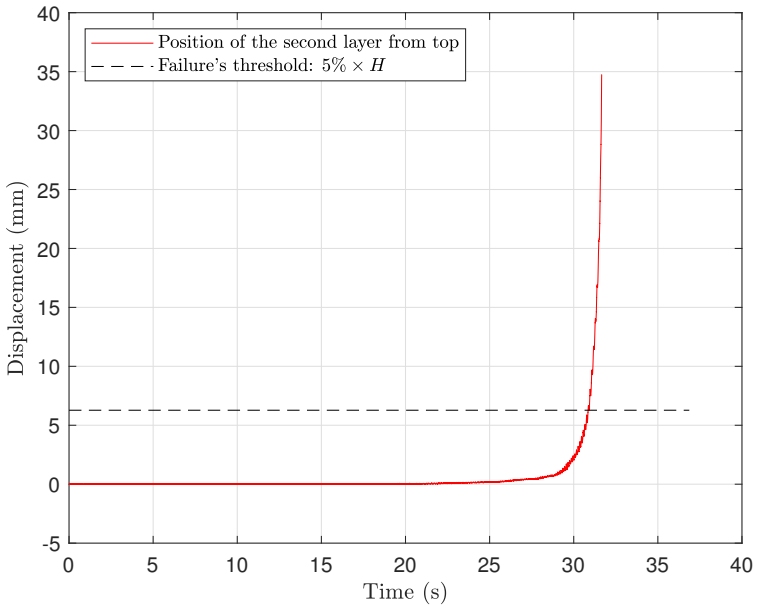

Figure 8. Displacement of the laser (pointing at the second to last row of bricks). Case of wall of height $H = 113$mm and width $B = 34$mm.

from past results. Indeed, in a previous study, Savalle et al. (2018a) showed that the interface friction angle can be related to the backfill internal friction angle φ'_{sand} through the relationship:

$$\frac{\delta_{\text{sand}}}{\varphi'_{\text{sand}}} = 0.71 \tag{6}$$

which is close to the common value of two third typically considered for this kind of interfaces. Thus, the interface friction angle δ_{sand} was such that:

$$\delta_{\text{sand}} = 0.71 * \varphi'_{\text{sand}} = 32^{\circ} \tag{7}$$

2.4. Analysis of the experimental data

To get back the acceleration corresponding to the triggering of the wall failure, both the data of the laser sensor (*Figure 2*) and the data of the harmonic waves are required. The laser sensor registered the displacement of the second row of bricks from top wall (an example is shown in *Figure 8*). The time t_{fail} associated to the wall failure has been defined as the time required to reach a given displacement threshold, herein defined as 5% of the wall height H (dashed line in *Figure 8*). This definition is consistent with the definition of Wu and Prakash (1996) who considered that an acceptable displacement for a rigid retaining wall is generally below 2% of its height, while a displacement characterising its failure is about 10% of it. In this study, the wall being discrete in nature, a smaller value of 5% was chosen as a limit value corresponding to failure.

Then, the amplitude A of the sinusoidal acceleration at time t_{fail} was found as a root mean square value of the imposed time-acceleration $S(t)$, recorded by ACC2, in a time window of duration $T = 1/f$ centred on t_{fail} (f being the frequency of the input signal used for the particular test: 10Hz, 30Hz, 50Hz or 70Hz)[4].

[4] $A = \sqrt{2 \times < \mathrm{S}^2(\mathrm{t}) >}$

The Version of Record of this manuscript has been published and is available in European Journal of Environmental and Civil Engineering. 24th November 2020.
DOI: http://www.tandfonline.com/10.1080/19648189.2020.1855477

Table 2. Repeatability tests: comparison of the accelerations at wall failure for identical tests. $g = 9.81\text{m.s}^{-2}$ refers to the natural gravity on earth.

	H/B = 3.3 H=11.3cm at 10Hz	H/B=2.3 H=7.9cm at 10Hz	H/B=2.3 H=7.9cm at 30Hz	H/B=2.3 H = 7.9cm at 50Hz	H/B=2.3 H=7.9cm at 70Hz
Test 1 (% g)	0.22	0.34	0.48	0.56	0.81
Test 2 (% g)	0.20	0.30	0.44	0.65	0.86
Test 3 (% g)	0.20	0.34	0.46	0.60	0.69
Mean acceleration (% g)	0.21	0.33	0.46	0.60	0.79
Standard deviation (% g)	0.02	0.02	0.02	0.04	0.09
Standard deviation (%)	8.1%	7.1%	4.1%	7.0%	11.2%

3. Experimental results

3.1. Repeatability of the tests

To have more insight into the repeatability of the experiments, two different walls (base width of 3.4cm and height equal to 7.9cm or 11.3cm) have been studied. Three identical tests were carried out for each of the signal frequencies of 10Hz, 30Hz, 50Hz and 70Hz for the wall of 7.9cm height following the protocol described in *Section 2.2.2*. This repeatability test was restricted to the frequency 10Hz for the wall with 11.3cm height. *Table 2* gives the acceleration at failure for all the repeatability tests. One can note that the tests are quite repeatable for all frequencies with a coefficient of variation of about 10%. The higher value of 11.2% was found for the imposed frequency signal of 70Hz. In the following, the study focuses on frequency 10Hz, as seismic frequencies are usually low: 10Hz in the model corresponds to actual seismic frequency of 2.2Hz (*Equation 4*).

3.2. Influence of H/B

The influence of the wall slenderness (i.e. its aspect ratio) on its dynamic resistance was first studied. Ten wall geometries with slenderness ranging from $H/B = 1.3$ to $H/B = 4.0$ have been tested. Nine of them had a base width of $B = 34$mm and various heights, ranging from $H = 44$mm to $H = 135$mm and one of them had a width of $B = 51$mm and a height of $H = 104$mm. *Figure 9* gives the results in terms of acceleration at failure time t_{fail}. A significant decrease of the wall dynamic resistance with respect to its slenderness can be observed, which was expected. The test with a thicker wall enabled to have arrangements of bricks with no full headers, which is more representative of actual arrangements in DSRWs. Its height was chosen in order to obtain a typical slenderness of $H/B = 2.0$. This first test (though needed to be confirmed by other tests) leads to the conclusion that slenderness is the main geometrical factor responsible for the dynamic resistance of dry-stack retaining walls, which has also been noticed for pseudo-static tests (Savalle et al., 2018a, 2018b). Moreover, the two typical failure modes of DSRWs were experimentally retrieved: sliding (crosses in *Figure 9*) occurred for the less slender walls whereas toppling (circles in *Figure 9*) occurred for the more slender ones. A mixed mode of failure was obtained for walls with slenderness ranging between 2 and 2.5 which is the typical range of actual DSRWs. *Figures 10 and 11* give snapshots of two walls through the development of toppling and sliding modes of failure. Generally, toppling was easier to identify compared to sliding since for the former type of failure, the wall kept a monolithic behavior until collapse. It was not the case for the sliding mode where local relative displacements occurred in different locations. Walls were considered to experience a sliding mode of failure when the top bricks slid and fell one by one until the total collapse of the retaining wall.

3.3. Influence of the motion frequency

In a second study, the influence of the frequencies of shakings has been investigated. For three different walls with three different slendernesses which are typical range of slendernesses of actual DSRWs ($H/B = 2.3$, $H/B = 2.7$ and $H/B = 3.3$), shaking table tests have been carried out for four signal frequencies 10Hz, 30Hz,

The Version of Record of this manuscript has been published and is available in European Journal of Environmental and Civil Engineering. 24th November 2020.
DOI: http://www.tandfonline.com/10.1080/19648189.2020.1855477

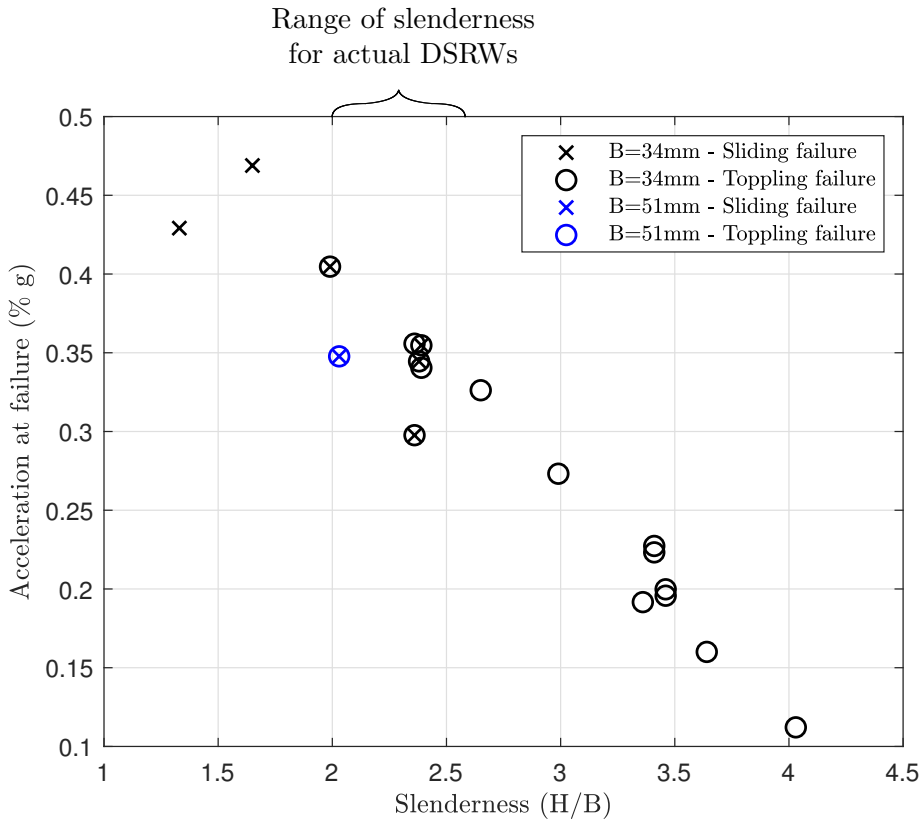

Figure 9. Acceleration at failure for the dry-joint brick retaining wall depending on its slenderness throughout experiments.

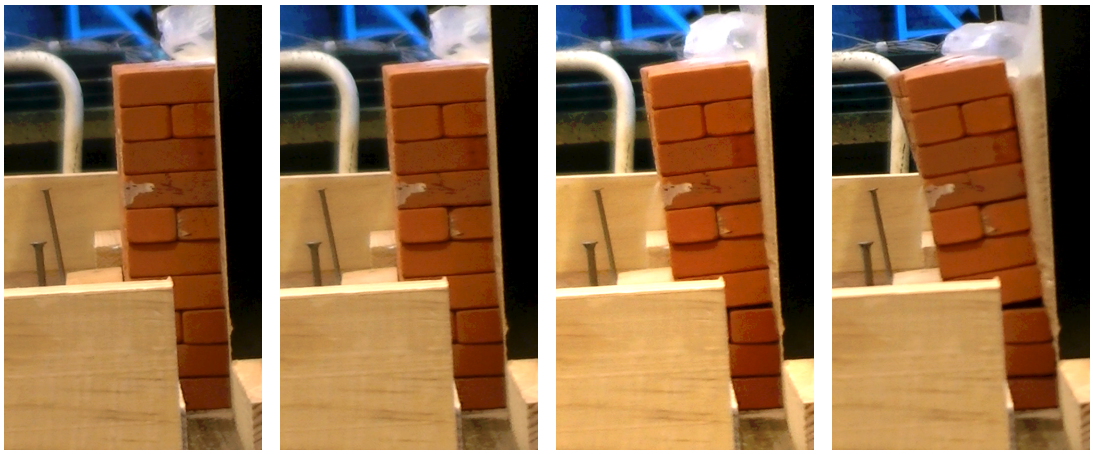

(a) (b) (c) (d)

Figure 10. Toppling mode of failure observed during the experiments. (a) to (d) show the evolution through time for one experiment.

The Version of Record of this manuscript has been published and is available in European Journal of Environmental and Civil Engineering. 24th November 2020.
DOI: http://www.tandfonline.com/10.1080/19648189.2020.1855477

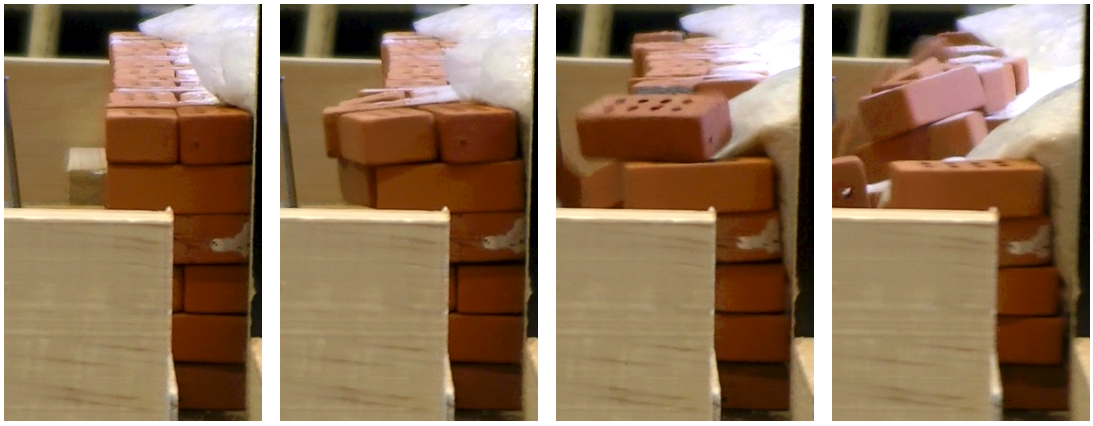

(a) (b) (c) (d)

Figure 11. Sliding mode of failure observed during the experiments. (a) to (d) show the evolution through time for one experiment.

50Hz and 70Hz. The results are shown in *Figure 12*, while full details can be found in the *Appendix A*. One can note that the walls resistance increases dramatically with the frequency of the base motion. Moreover, for the slenderness of 3.3, the mode of failure was found independent of the signal frequency. It is not the case for the two other studied slendernesses which were smaller and where sliding was generally triggered for higher frequencies. As previously mentioned, sliding generally occurs with local failures of bricks. However for slenderness $H/B = 2.7$ and frequency 70Hz, a monolithic slide started to occur at the bottom right corner wall and then a toppling mode of failure propagated through the wall (*Figure 13*). One could note that this failure did not develop following plane strain assumptions, on the contrary to the vast majority of toppling failed walls. This can easily be explained by local material and geometrical heterogeneities, and especially at the two ends, leading to more vulnerable parts.

The increase of resistance with the frequency may be linked to the following points:

- The duration of each cycle of loading is shorter (though more frequent),
- The velocity amplitude is smaller; indeed the Peak Ground Velocity (PGV) is known to be a relevant parameter to caracterised the destructive power of a seismic loading (Richards & Elms, 1979),
- The maximum dynamic earth pressure is lower due to the decrease of the wave length of the input signal with the increase of the frequency (Baziar et al., 2013; Bellezza, 2014; Pain et al., 2015). Indeed, though at $f = 10$Hz, the wave length is approximately equal to $\lambda = \frac{C_s}{f} \approx 6$m which is much larger than the wall height ($H \approx 10$cm), at $f = 70$Hz, the wave length decreases to $\lambda \approx 0.9$m]. For a wall of height $H \approx 10$cm, the local dynamic earth pressure may not be any more constant along its height.
- The smaller displacements (at each cycle, as well as total displacements) are more endurable by the structure.

To illustrate this latter point, the author propose hereafter an analysis of a single brick based on Newmark's theory (Newmark, 1965). Newmark's analysis is here intended as a explaining tool for the increase of failure acceleration with the increase of the frequency of the base motion. Basically, Newmark's theory consists in integrating twice the acceleration record. Therefore, it leads to a displacement amplitude divided by ω^2 (ω being the angular frequency in rad/s), compared to the acceleration amplitude. In order to obtain the total displacement, we sum the displacements occurring for each cycle, thus multiplying one cycle's displacement by the number of cycles, which is proportional to the angular frequency ω. In the end, the total displacement is inversely proportional to the frequency f of the base motion. The following developments give complementary details.

For the sake of simplicity and in a context where just qualitative results are expected, a very basic modelling is chosen, neglecting for instance the earth pressure. The analysis is focused on the stability of one brick of the last layer, since it has been observed that in case of sliding failures, bricks of the topmost layer fell the first. The pseudo-static critical acceleration a_{max} is taken as the tangent of the brick-brick friction angle. Then, a Newmark's scheme is adopted, where at every moment the input acceleration $S(t)$ is bigger than the threshold $a_{max} = g * \tan(\varphi'_{brick})$, the total displacement of the studied brick d is computed with a Matlab home code

The Version of Record of this manuscript has been published and is available in European Journal of Environmental and Civil Engineering. 24th November 2020.
DOI: http://www.tandfonline.com/10.1080/19648189.2020.1855477

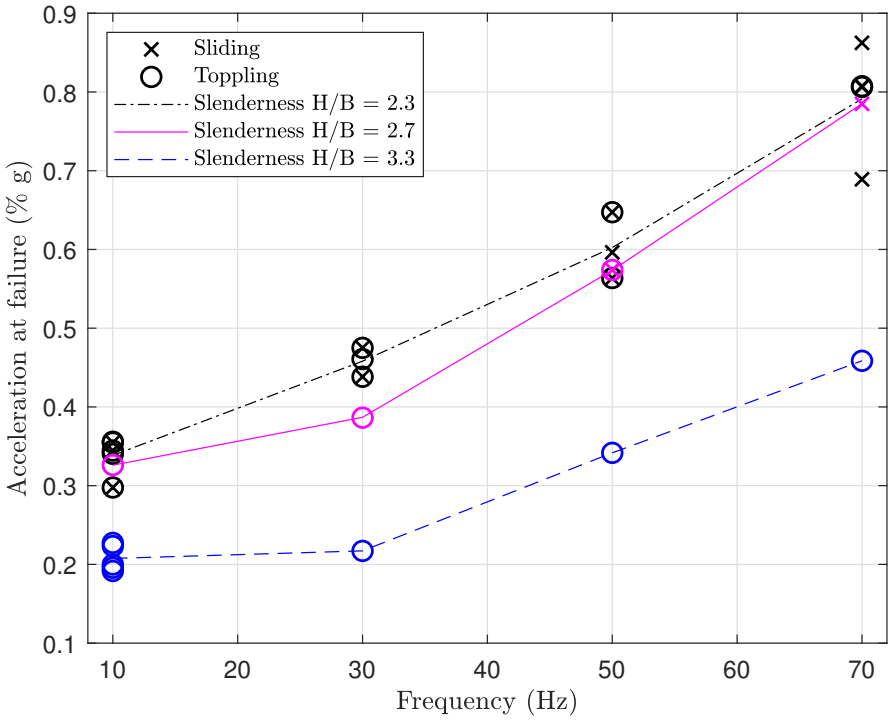

Figure 12. Influence of the frequency on the acceleration at failure for three different walls.

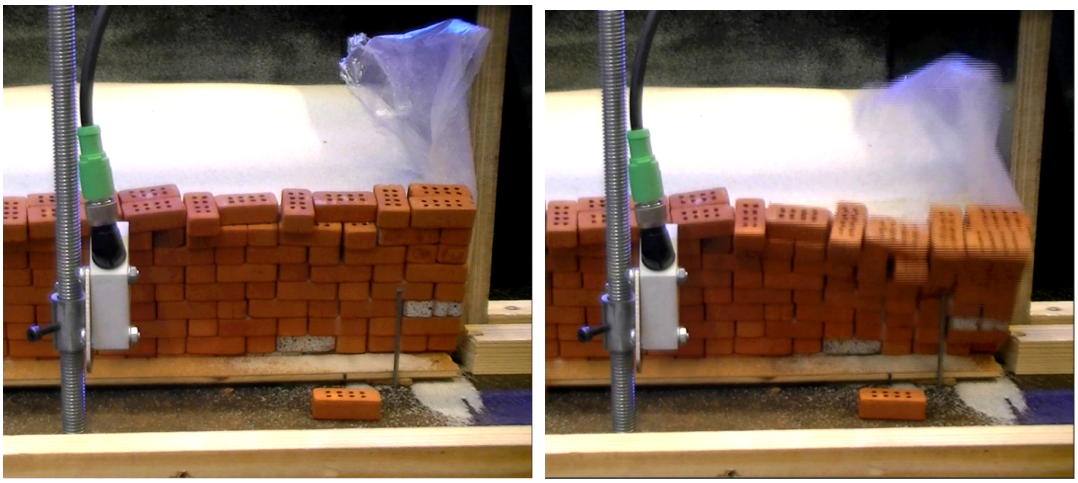

(a) Trigerring of a sliding failure (b) Toppling failure

Figure 13. Special feature of failure for the wall $H/B = 2.67$ at 70Hz. (a) First, the wall slides at its bottom right corner. (b) Then, a toppling failure is triggered and propagates through the wall.

The Version of Record of this manuscript has been published and is available in European Journal of Environmental and Civil Engineering. 24th November 2020.
DOI: http://www.tandfonline.com/10.1080/19648189.2020.1855477

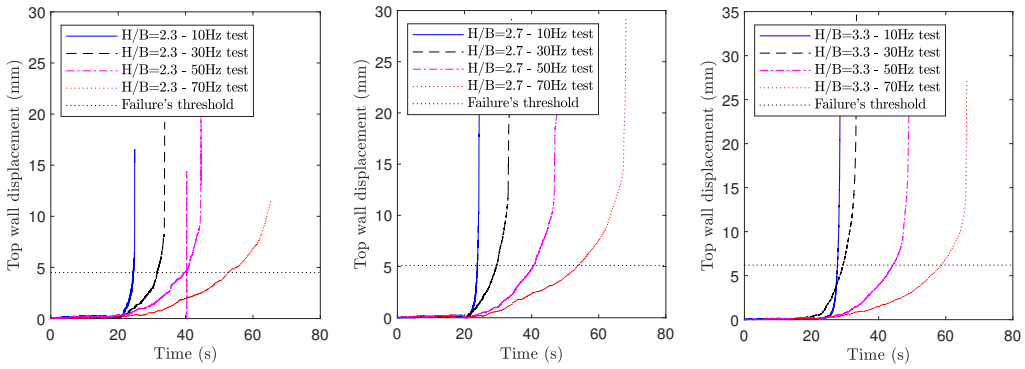

(a) Displacement for $H/B = 2.3$ (b) Displacement for $H/B = 2.7$ (c) Displacement for $H/B = 3.3$

Figure 14. Displacement curves of the three walls ($H/B \in [2.3;\ 2.7;\ 3.3]$) shaken by input signals using the four frequencies (10, 30, 50 and 70Hz).

integrating twice the unbalanced acceleration $S(t) - a_{max}$. Since the brick can only move if the acceleration is directed outward, the double integration is carried out only for $S(t) > a_{max}$ and not for $S(t) < -a_{max}$. Using the parameters of the experiments (*Equation 5* with $a_{max} = 0.62g$ and $A = 1.0g\ \mathrm{s}^{-1}$), one can obtain the following fitted relationship:

$$d = 0.18 \times \frac{(t - 33)^{2.75}}{f} \tag{8}$$

with f the frequency of the signal and t the reference time of the test. The numeric values (0.18, 33 and 2.75) enable to fit the original curve, which basically contains steps associated to stable phases. These numerical values depend on the parameters a_{max} and A, though no simple relationships have been found. One could notice however that using constant amplitude harmonic signal, the value *33* is replaced by *0* and the *2.75* one is replaced by *1*.

During the experiments, the failure has been detected through a displacement criteria $d_{crit} = 5\% * H$. Then, inverting *Equation 8* for a given wall height H, one can find that the failure time t_{fail} is a root function of the frequency f of the input. Therefore, it partially explains why sliding failures were triggered later for higher frequency inputs.

In *Figure 14*, the displacements measured throughout the tests for the three walls subjected to the four frequency input signals have been plotted. Firstly, it is noted that irrespective of the frequency, noticeable wall displacement (above 1mm) occur at the same moment, i.e. at the same acceleration level. Therefore, until a certain acceleration level, the input frequency does not play a significant role: the dynamic behaviour of the wall is not yet mobilised. This acceleration threshold only depends on the wall's static resistance and is slightly higher than the pseudo-static resistance of the wall. Secondly, the rate of increase of the displacement through time is slower for higher frequencies. In addition, one can note that though the wall shaken by 10Hz harmonic waves can indeed be considered as near collapsing when reaching the 5% displacement threshold, this is not the case when it is shaken with higher frequency signals. In fact, the behaviour of the wall shaken by 10Hz waves is a rigid one with no displacement in a first phase until a threshold after which huge displacements and brittle failure occur. Conversely, the larger the frequency is, the more ductile its response seems to be: walls can handle huge displacements without collapsing and these displacements are noticeable well before the wall collapse. This capacity to experience stable irreversible displacements is clearly linked to the capacity of the wall to dissipate seismic energy, and thus to resist to an earthquake. This is particularly interesting for actual DSRWs, where their actual resistance could be much higher than the one evaluated through classical pseudo-static approaches.

To conclude, the retaining wall seems to be less vulnerable to higher frequencies. This extra resistance is permitted by small and stable relative movements of the bricks and/or the whole wall. These ones are irreversible, enabling to dissipate the energy of the input signal. Analysing again the experimental results of Huang et al. (2010), sand slopes seem also to be more resistant to higher frequency motions, though this had not been highlighted by the authors. Huang et al. (2010) carried out shaking-table tests on three identical sand slopes using tapered input waves of growing amplitude. The three sand slopes were subjected to three different frequency waves: 3Hz, 6Hz and 15Hz. From *Figure 6* of their article, it appears that higher frequency tapered waves were required to trigger the slope failure.

The Version of Record of this manuscript has been published and is available in European Journal of Environmental and Civil Engineering. 24th November 2020.
DOI: http://www.tandfonline.com/10.1080/19648189.2020.1855477

Table 3. Comparison between resistance to 10Hz harmonic motion and pseudo-static resistance of dry-joint walls depending on the slenderness of the wall. The failure mode, sliding (S) or toppling (T), is also depicted.

Slenderness of the wall (H/B)	Relative difference (gap in %)	Failure mode
1.3	0%	S
1.7	16%	S
2.0	12%	S/T
2.3	18%	S/T
2.7	43%	T
3.0	51%	T
3.3	45%	T
3.7	44%	T
4.0	34%	T
Mean value	29%	-

3.4. Comparison with a pseudo-static study

The results obtained throughout the experimental dynamic tests have been compared to results obtained throughout a pseudo-static approach of the problem in order to evaluate how much this latter is conservative. The pseudo-static method considered herein is based on the limit equilibrium of a Coulomb's wedge of soil, that includes the pseudo-static force modelling the seismic action. Then, the stability of the wall is checked according to two possible modes of failure, sliding and toppling. This method has been validated on pseudo-static experiments (Savalle et al., 2018a).

Table 3 gives the relative difference, denoted *gap*, between the acceleration at failure for the dynamic approach (for 10Hz input signals) and the one derived analytically from the pseudo-static approach according to the wall slenderness.

$$gap = \frac{\mathrm{acc}_{\mathrm{dynamic}}(10\mathrm{Hz}) - \mathrm{acc}_{\mathrm{pseudo-static}}}{\mathrm{acc}_{\mathrm{pseudo-static}}} \tag{9}$$

First, the results confirm that the pseudo-static approach (which is equivalent to a 0Hz frequency input motion) is generally conservative since almost only positive values were obtained. The special case where slenderness is equal to 1.3 should require more tests before confirmation. When the walls tended to fail by toppling (high slendernesses), the relative difference lies around 45%, which is very significant. On the other hand, when the walls tended to fail by sliding (low slendernesses), the relative difference falls down to 15%. Typical slendernesses for DSRWs ranges between $H/B = 2$ and $H/B = 2.7$ where the relative difference decreased from 43% to 12%. Then, depending on the properties of the studied DSRW, a pseudo-static approach could be just conservative or very conservative.

In fact, these experimental results have to be analysed in the light of the conclusions made previously:

- Increasing the frequency of the motion increases the resistance of a dry-joint retaining wall, and since natural seismic motions usually have a frequency content that extends beyond the frequency of 2.2Hz (equivalent to the 10Hz frequency input in the shaking-table tests), the relative difference *gap* may be most of the time higher than those noted in *Table 3* (*Table 4*).
- From some other tests not shown here, it has been noted that the larger the duration of the base motion was, the lower the wall's resistance was. Earthquakes often last less than 30 seconds, which is the average duration of the harmonic input used herein. Therefore, the actual seismic resistance of slope DSRWs may probably be higher than that identified in this work.

Finally, a seismic behaviour coefficient $r = 1.2$ can be proposed from the present experimental campaign. This can already be used in conjunction with a pseudo-static approach. As explained above, this value can still be considered as too conservative in many cases. Therefore, further numerical simulations involving true seismic motions would be helpful to support a higher value for this coefficient. On the other hand, one could conduct Newmark's analysis on the displacement of the retaining wall, as it is commonly performed for geosynthetic

The Version of Record of this manuscript has been published and is available in European Journal of Environmental and Civil Engineering. 24th November 2020.
DOI: http://www.tandfonline.com/10.1080/19648189.2020.1855477

Table 4. Comparison between resistance to harmonic motion of varying frequency and pseudo-static resistance of dry-joint walls of slenderness H/B = 2.3.

Frequency of the test (Hz)	Relative difference e (%)
10	18%
30	60%
50	110%
70	176%

reinforced earth retaining walls (Masini et al., 2015; Gaudio et al., 2018). For these particular systems, since it has been found that the failure mode predicted by pseudo-static analysis was similar to the one developed throughout dynamic simulations (Masini et al., 2015), pseudo-static methods can be very efficient for an in-field application, since less time-consuming than dynamic simulations. However, back to DSRWs, the validity of Newmark's analysis for this class of retaining walls still needs to be demonstrated, and above all regarding the ability of Newmark's method to handle toppling failure modes.

4. Conclusion

The seismic behaviour of slope dry stone retaining walls has been studied through a simplified case of harmonic shaking-table tests where the input acceleration is a sinus associated to a single frequency. Experiments have been carried out on a model of actual dry stone retaining walls composed of parallelepiped bricks. Their resistance to shaking have been investigated for input signals of increasing amplitude, with different harmonics.

As expected, their resistance was found decreasing with slenderness. Classical toppling failures have been observed for slender walls, while less slender ones experienced local failures of bricks that could be akin to a sliding failure. As long as the frequency of the harmonic input wave increases, the wall's resistance increases as well and the toppling mode of failure is progressively replaced by sliding ones. It has been noted that a dry-stack retaining wall can experience small local relative displacements throughout the shaking, particularly when subjected to higher frequency motions. It may be an advantage since relative displacements contribute to dissipate energy. Based on these experimental results and on a pseudo-static approach, the seismic behaviour coefficient has been derived for the experimental walls. A reasonable value of $r = 1.2$ can be selected for a pseudo-static analysis of DSRWs. Finally, this experimental campaign paves the way for future studies in the field, either for numerical computations furnishing a complete, detailed and wide experimental data set. It also sets the basis for similar experiments with a consolidated and accurate protocol.

To conclude, the contribution of the paper to the field can be summarised as follows:

(1) It provides the first experimental data set of shaking-table tests involving dry-stack masonry retaining walls, which will be helpful for numerical validations. It should lead to a better understanding of the seismic behaviour of Dry Stone Retaining Walls (DSRWs).

(2) It gives details about the best way to conduct shaking-table tests on retaining structures with high reproducibility, with some insights about the way to handle a densifying backfill or to identify the internal friction angle of a low confined sand.

(3) It brings to light the capacity of dry-stack retaining walls to experience small stable relative movements, and especially when the frequency of the input signal is high. It leads to a greater seismic capacity of walls for higher frequencies.

(4) It evidences that for a given wall, irrespective of the frequency of the base motion, noticeable displacements starts to occur for the same acceleration threshold.

(5) It identifies a first and conservative seismic behaviour coefficient for pseudo-static studies of DSRWs, which is equal to 1.2. This behaviour coefficient is generally sensitive to the wall slenderness, the duration of the motion or the frequency content.

The Version of Record of this manuscript has been published and is available in European Journal of Environmental and Civil Engineering. 24th November 2020.
DOI: http://www.tandfonline.com/10.1080/19648189.2020.1855477

Acknowledgements

The authors want to thank the French Ministry of Higher Education and Research for their financial support through the PhD scholarship. The authors want also to acknowledge the support of the technical team of the ENTPE, and particularly the help of Stéphane COINTET. The authors valued a lot the conversations had with Dr. Thiep DOANH and Dr. Denis BRANQUE (ENTPE) in relation to the behaviour of sands at low confining pressures.

References

Alejano, L. R., Veiga, M., Gómez-Márquez, I., & Taboada, J. (2012). Stability of granite drystone masonry retaining walls: II. Relevant parameters and analytical and numerical studies of real walls. *Géotechnique*, *62*(11), 1027–1040.

Alejano, L. R., Veiga, M., Taboada, J., & Díez-Farto, M. (2012). Stability of granite drystone masonry retaining walls: I. Analytical design. *Géotechnique*, *62*(11), 1013 –1025.

Alshibli, K. A., Batiste, S. N., & Sture, S. (2003). Strain localization in sand: plane strain versus triaxial compression. *Journal of Geotechnical and Geoenvironmental Engineering*, *129*(6), 483–494.

Amirouche, N. (2008). *Dispositifs absorbants à base de matériaux à double porosité dans des champs acoustiques complexes* (PhD Thesis). ENTPE, DGCB.

Bathurst, R. J. (2002). Shaking table model study on the dynamic response of reinforced soil walls. In *Proc. 7th Int. Geosynthetic Conf., Nice, France, 2002* (Vol. 1, pp. 99–102).

Bathurst, R. J., Hatami, K., & AlfaroI, M. C. (2002). Geosynthetic-reinforced soil walls and slopes—seismic aspects. *Geosynthetics and their applications*, 327-392.

Baziar, M. H., Shahnazari, H., & Moghadam, M. R. (2013). Sliding stability analysis of gravity retaining walls using the pseudo-dynamic method. *Geotechnical Engineering*, *166*(4), 389–398.

Bellezza, I. (2014). A New Pseudo-dynamic Approach for Seismic Active Soil Thrust. *Geotechnical and Geological Engineering*, *32*(2), 561–576.

Biarez, J., & Hicher, P.-Y. (1994). *Elementary mechanics of soil behaviour: saturated remoulded soils.* AA Balkema.

Bolton, M. D. (1986). The strength and dilatancy of sands. *Géotechnique*, *36*(1), 65–78.

Burgoyne, J. (1853). Revetments of retaining walls. *Corps of Royal Engineers Papers*, *3*, 154–159.

CAPEB, ABPS, Muraillers-de-Provence, CBPS, CMA84, & ENTPE. (2008). *Pierres sèches : guide de bonnes pratiques de construction de murs de soutènement.* ENTPE.

Capper, P. L., & Cassie, W. F. (1969). *The mechanics of engineering soils.* The national academy of science engineering medicine.

Chakraborty, T., & Salgado, R. (2009). Dilatancy and shear strength behavior of sand at low confining pressures. In *Proceedings of the 17th international conference on soil mechanics and geotechnical engineering: The academia and practice of geotechnical engineering* (pp. 652–655).

Claxton, M., Hart, R. A., McCombie, P. F., & Walker, P. J. (2005). Rigid block distinct-element modelling of dry-stone retaining walls in plane strain. *ASCE Journal of Geotechnical and Geoenvironmental Engineering*, *131*(3), 381–389.

The Version of Record of this manuscript has been published and is available in European Journal of Environmental and Civil Engineering. 24th November 2020.
DOI: http://www.tandfonline.com/10.1080/19648189.2020.1855477

Clayton, C. R., Woods, R. I., Bond, A. J., & Milititsky, J. (2014). *Earth pressure and earth-retaining structures*. CRC Press.

Colas, A.-S., Morel, J.-C., & Garnier, D. (2008). Yield design of dry-stone masonry retaining structures - Comparisons with analytical, numerical, and experimental data. *International Journal for Numerical and Analytical Methods in Geomechanics*, *32*(14), 1817–1832.

Colas, A.-S., Morel, J.-C., & Garnier, D. (2010). Full-scale field trials to assess dry-stone retaining wall stability. *Engineering Structures*, *32*(5), 1215–1222.

Colas, A.-S., Morel, J.-C., & Garnier, D. (2013a). Assessing the two-dimensional behaviour of drystone retaining walls by full-scale experiments and yield design simulation. *Géotechnique*, *63*(2), 107–117.

Colas, A.-S., Morel, J.-C., & Garnier, D. (2013b). Yield design modelling of dry joint retaining structures. *Construction and Building Materials*, *41*, 912–917.

Combe, A.-L. (1998). *Comportement du sable d'Hostun S28 au triaxial axisymétrique. Comparaison avec le sable d'Hostun RF* (MA Thesis).

Dewoolkar, M. M., Ko, H.-Y., & Pak, R. Y. S. (2000). Experimental developments for studying static and seismic behavior of retaining walls with liquefiable backfills. *Soil Dynamics and Earthquake Engineering*, *19*(8), 583–593.

Dickens, J. G., & Walker, P. J. (1996). Use of distinct element model to simulate behaviour of dry-stone walls. *Structural Engineering Review*, *2-3*(8), 187–199.

ENTPE, ABPS, Ecole-des-Ponts-ParisTech, IFSTTAR, & FFB. (2017). *Technique de construction des murs en pierre sèche : Règles professionnelles*. ENTPE, ABPS.

Fairless, G. J. (1989). *Seismic performance of reinforced earth walls* (PhD Thesis). University of Canterbury.

Fukumoto, Y., Yoshida, J., Sakaguchi, H., & Murakami, A. (2014). The effects of block shape on the seismic behavior of dry-stone masonry retaining walls: A numerical investigation by discrete element modeling. *Soils and Foundations*, *54*(6), 1117–1126.

Gaudio, D., Masini, L., & Rampello, S. (2018). A performance-based approach to design reinforced-earth retaining walls. *Geotextiles and Geomembranes*, *46*(4), 470–485.

Harkness, R. M., Powrie, W., Zhang, X., Brady, K. C., & M.P. O'Reilly. (2000). Numerical modelling of full-scale tests on drystone masonry retaining walls. *Géotechnique*, *50*(2), 165–179.

Huang, C.-C., Horng, J.-C., Chang, W.-J., Chueh, S.-Y., Chiou, J.-S., & Chen, C.-H. (2010, August). Dynamic behavior of reinforced slopes: horizontal acceleration response. *Geosynthetics International*, *17*(4), 207–219.

Huang, C.-C., Wu, S.-H., & Wu, H.-J. (2009, January). Seismic Displacement Criterion for Soil Retaining Walls Based on Soil Strength Mobilization. *Journal of Geotechnical and Geoenvironmental Engineering*, *135*(1), 74–83.

Husband, J., & Harby, W. (1911). *Structural engineering*. Longmans, Green, and Company.

Iai, S. (1989). Similitude for shaking table tests on soil-structure-fluid model in 1g gravitational field. *Soils and Foundations*, *29*(1), 105–118.

Ishibashi, I., & Fang, Y.-S. (1987). Dynamic earth pressures with different wall movement modes. *Soils and Foundations*, *27*(4), 11–22.

Koseki, J., Munaf, Y., Sato, T., Tatsuoka, F., Tateyama, M., & Kojima, K. (1998). Shaking and tilt table tests of geosynthetic-reinforced soil and conventional-type retaining walls. *Geosynthetics International*, *5*(1-2), 73–96.

The Version of Record of this manuscript has been published and is available in European Journal of Environmental and Civil Engineering. 24th November 2020.
DOI: http://www.tandfonline.com/10.1080/19648189.2020.1855477

Krawinkler, H. (1988). Scale effects in static and dynamic model testing of structures. In *Proceedings of the Ninth World Conference on Earthquake Engineering, Tokyo, Japan* (pp. 2–9).

Lancelot, L., Shahrour, I., & Al Mahmoud, M. (1996). Comportement du sable d'Hostun sous faibles contraintes. *Revue Française de Géotechnique*(74), 63–74.

Le, H. H., Garnier, D., Colas, A.-S., Terrade, B., & Morel, J.-C. (2016). 3d homogenised strength criterion for masonry: Application to drystone retaining walls. *Journal of the Mechanics and Physics of Solids*, *95*, 239–253.

Le, H. H., Morel, J.-C., Colas, A.-S., Terrade, B., & Garnier, D. (2019). Assessing the three-dimensional behaviour of dry stone retaining walls by full-scale experiments. *International Journal of Architectural Heritage*, 1–11.

Lo Grasso, A. S., Maugeri, M., & Recalcati, P. (2004). Shaking table tests and analysis of reinforced slopes. In *Proc. Of The Geoasia 2004 Conference, Seoul* (pp. 21–23).

Maksimovic, M. (1989). Nonlinear failure envelope for soils. *Journal of Geotechnical Engineering*, *115*(4), 581–586.

Masini, L., Callisto, L., & Rampello, S. (2015). An interpretation of the seismic behaviour of reinforced-earth retaining structures. In *Geotechnical Earthquake Engineering: Géotechnique Symposium in Print 2015* (pp. 25–34). ICE Publishing.

McCombie, P. F., Mundell, C., Heath, A., & Walker, P. (2012). Drystone retaining walls: Ductile engineering structures with tensile strength. *Engineering Structures*, *45*, 238–243.

Mundell, C., McCombie, P., Bailey, C., Heath, A., & Walker, P. (2009). Limit-equilibrium assessment of drystone retaining structures. *Proceedings of the Institution of Civil Engineers (Geotechnical Engineering)*, *162*(4), 203–212.

Mundell, C., McCombie, P., Heath, A., & Harkness, J. (2010). Behaviour of drystone retaining structures. *Proceedings of the Institution of Civil Engineers (Structures and Building)*, *163*(1), 3–12.

Newmark, N. M. (1965). Effects of earthquakes on dams and embankments. *Géotechnique*, *15*(2), 139–160.

Oetomo, J. J., Vincens, E., Dedecker, F., & Morel, J.-C. (2016). Modeling the 2d behavior of dry-stone retaining walls by a fully discrete element method. *International Journal for Numerical and Analytical Methods in Geomechanics*, *40*(7), 1099–1120.

Pain, A., Choudhury, D., & Bhattacharyya, S. K. (2015). Seismic stability of retaining wall–soil sliding interaction using modified pseudo-dynamic method. *Géotechnique Letters*, *5*(1), 56–61.

Powrie, W., Harkness, R. M., Zhang, X., & Bush, D. I. (2002). Deformation and failure modes of drystone retaining walls. *Géotechnique*, *52*(6), 435–446.

Pulatsu, B., Kim, S., Erdogmus, E., & Lourenço, P. B. (2020). Advanced analysis of masonry retaining walls using mixed discrete–continuum approach. *Proceedings of the Institution of Civil Engineers-Geotechnical Engineering*, 1–13.

Quezada, J.-C., Vincens, E., Mouterde, R., & Morel, J.-C. (2016). 3d failure of a scale-down dry stone retaining wall : a DEM modelling. *Engineering Structures*, *117*, 506–517.

Richards, R., & Elms, D. G. (1979). Seismic Behavior of Gravity Retaining Walls. *Journal Of The Geotechnical Engineering Division*, *105*(4), 449–464.

The Version of Record of this manuscript has been published and is available in European Journal of Environmental and Civil Engineering. 24th November 2020.
DOI: http://www.tandfonline.com/10.1080/19648189.2020.1855477

Savalle, N. (2019). *Comportement sismique des murs de soutènement de talus en pierre sèche* (PhD Thesis). Lyon.

Savalle, N., Vincens, E., & Hans, S. (2018a). Pseudo-static scaled-down experiments on dry stone retaining walls: Preliminary implications for the seismic design. *Engineering Structures*, *171*, 336–347.

Savalle, N., Vincens, E., & Hans, S. (2018b). Seismic behaviour of dry stone retaining walls: experimental and numerical pseudo-static studies. In *10th International Masonry Conference (IMC), Milan* (pp. 1030–1045). Milan.

Savalle, N., Vincens, E., & Hans, S. (2020). Experimental and numerical studies on scaled-down dry-joint retaining walls: Pseudo-static approach to quantify the resistance of a dry-joint brick retaining wall. *Bulletin of Earthquake Engineering*, *18*(2), 581–606.

Srilatha, N., Latha, G. M., & Puttappa, C. G. (2013). Effect of frequency on seismic response of reinforced soil slopes in shaking table tests. *Geotextiles and Geomembranes*, *36*, 27–32.

Sture, S., Costes, N. C., Batiste, S. N., Lankton, M. R., AlShibli, K. A., Jeremic, B., ... Frank, M. (1998). Mechanics of granular materials at low effective stresses. *Journal of Aerospace Engineering*, *11*(3), 67–72.

Sugimoto, M., Ogawa, S., & Moriyama, M. (1994). Dynamic characteristics of reinforced embankments with steep slope by shaking model tests. In *Recent Case Histories of Permanent Geosynthetic-Reinforced Soil Walls, Seiken Symposium* (pp. 271–275).

Terrade, B., Colas, A.-S., & Garnier, D. (2018). Upper bound limit analysis of masonry retaining walls using PIV velocity fields. *Meccanica*, *53*(7), 1661–1672.

Villemus, B., Morel, J.-C., & Boutin, C. (2006). Experimental assessment of dry stone retaining wall stability on a rigid foundation. *Engineering Structures*, *29*(9), 2124–2132.

Walker, P., & Dickens, J. G. (1995). Stability of medieval dry stone walls in Zimbabwe. *Géotechnique*, *45*(1), 141–147.

Walker, P., McCombie, P., & Claxton, M. (2007). Plane strain numerical model for drystone retaining walls. *Proceedings of the Institution of Civil Engineers - Geotechnical Engineering*, *160*(2), 97–103.

Wilson, P., & Elgamal, A. (2015). Shake table lateral earth pressure testing with dense c-ϕ backfill. *Soil Dynamics and Earthquake Engineering*, *71*, 13–26.

Wu, Y., & Prakash, S. (1996). On seismic displacements of rigid retaining walls. In *Analysis and design of retaining structures against earthquakes* (pp. 21–37).

The Version of Record of this manuscript has been published and is available in European Journal of Environmental and Civil Engineering. 24th November 2020.
DOI: http://www.tandfonline.com/10.1080/19648189.2020.1855477

5. Appendices

Appendix A. Ending acceleration of shaking-table tests

In this appendix the test protocol is more detailed. The nominal test, whose a full record is given in *Figure A1*, lasted 1 min (from 0.01% g to 1.02% g), with the failure occurring approximately around 30 seconds. However, the ending acceleration of the shaking was varying depending on the wall's expected resistance. *Table A1* sums up the ending accelerations of each test depending on the aspect ratio (H/B) of the wall. The relatively short duration of each test enables further numerical simulations of the experiments. Similarly, full details of the tests carried out using different frequencies are given in *Table A2*. In this table, the duration refers to the duration between the beginning of the test and the failure of the wall, including the 5 seconds of automatic calibration of the shaking-table at low-level shaking (*Figure A1*).

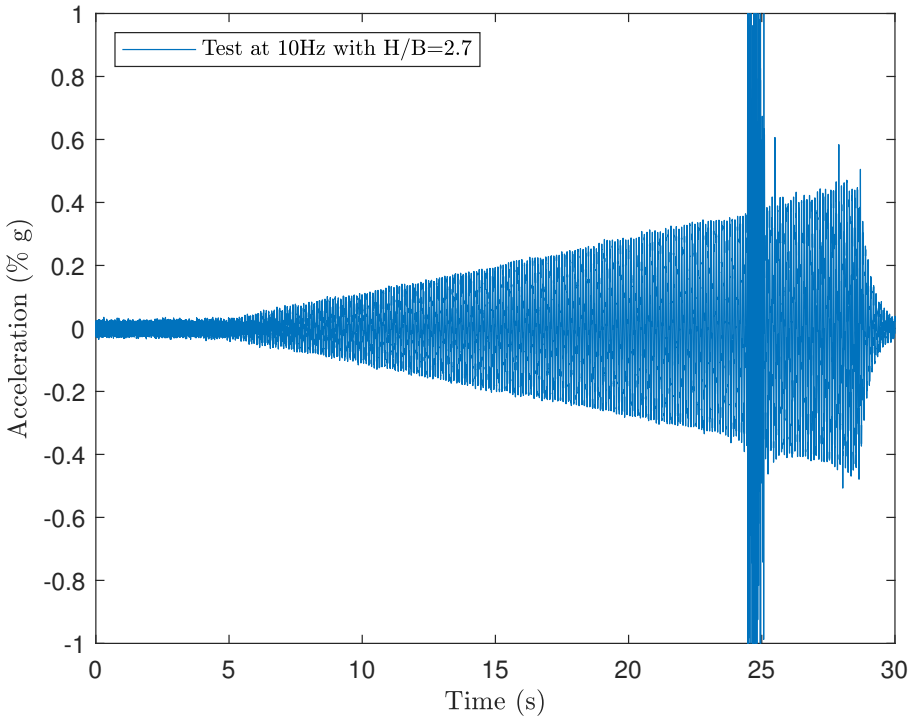

Figure A1. Example of a typical acceleration record used during the experiments. First phase (before $t = 5$s) corresponds to the automatic calibration of the shaking-table. Then, the acceleration is linearly growing during the second phase. At around $t = 25$s, the wall collapses, generating huge noise in the acceleration record. Finally, the test is manually stopped at $t = 29$s.

Appendix B. Evaluation of the friction angle of the sand

In this appendix, the authors sum up a literature analysis on friction angle of low confined sand, with the aim of having some reference values. Sands are known for increasing their friction angle as confining pressure decreases (Lancelot et al., 1996). Some analytical formulas (Bolton, 1986; Maksimovic, 1989) have been calibrated on low-pressure experiments (Lancelot et al., 1996) involving Hostun RF sand, which is very close to Hostun S28 sand used in the present work (Combe, 1998). Some analytical equations have also been calibrated on experimental results for Toyoura sand (Chakraborty & Salgado, 2009). Finally, very low-pressure tests have been conducted out of gravity on Ottawa sand (Sture et al., 1998; Alshibli et al., 2003). All the results from these studies are gathered in *Table B1*, leading to values well above $\varphi'_{sand} = 50°$. From these results, the value found by the authors of $\varphi'_{sand} = 45°$ is plausible.

The Version of Record of this manuscript has been published and is available in European Journal of Environmental and Civil Engineering. 24th November 2020.
DOI: http://www.tandfonline.com/10.1080/19648189.2020.1855477

Table A1. Ending accelerations of the shaking-table tests.

Slenderness of the wall	Ending acceleration (% g)
1.3	15
1.7	10
2.0	10
2.3	10
2.7	10
3.0	5
3.3	5
3.7	3
4.0	2

Table A2. Complementary details of the experimental tests carried out using different frequencies: duration and failure acceleration.

Slenderness of the wall (H/B)	Frequency (Hz)	Duration (s)	Failure acceleration (% g)
2.3	10	25	0.34
		25	0.34
		22	0.30
	30	33	0.47
		30	0.44
		32	0.46
	50	38	0.56
		43	0.65
		40	0.60
	70	53	0.81
		46	0.69
		56	0.86
2.7	10	24	0.33
	30	30	0.39
	50	41	0.57
	70	54	0.78
3.3	10	31	0.22
		28	0.20
		27	0.20
	30	29	0.22
	50	44	0.34
	70	59	0.46

The Version of Record of this manuscript has been published and is available in European Journal of Environmental and Civil Engineering. 24th November 2020.
DOI: http://www.tandfonline.com/10.1080/19648189.2020.1855477

Table B1. Friction angle of dense sands at very low confining pressure according to the literature (Bolton, 1986; Maksimovic, 1989; Lancelot et al., 1996; Sture et al., 1998; Alshibli et al., 2003; Chakraborty & Salgado, 2009). For analytical expression, these values were derived using $p' = 0.7$kPa, as it was the mean pressure along the experiments.

Authors	Type	Sand	φ' (°)	Comments
(Lancelot et al., 1996) and (Maksimovic, 1989)	Anal.	Hostun RF	55°	validated up to a minimum pressure of 20kPa
(Lancelot et al., 1996) and (Bolton, 1986)	Anal.	Hostun RF	55°	validated up to a minimum pressure of 20kPa
(Chakraborty & Salgado, 2009)	Anal.	Toyoura	53°	validated up to a minimum pressure of 4kPa
(Sture et al., 1998) (Alshibli et al., 2003)	Exp.	Ottawa	54°	Mean from two tests at 0.52kPa. Friction rapidly dropped from 1% strain reaching 38° at 5% strain